ADVANCED MATERIALS
www.advmat.de

Combinatorial Strategy for Studying Biochemical Pathways in Double Emulsion Templated Cell-Sized Compartments

Elena C. dos Santos, Andrea Belluati, Danut Necula, Dominik Scherrer, Claire E. Meyer, Riccardo P. Wehr, Emanuel Lörtscher, Cornelia G. Palivan, and Wolfgang Meier**

Cells rely upon producing enzymes at precise rates and stoichiometry for maximizing functionalities. The reasons for this optimal control are unknown, primarily because of the interconnectivity of the enzymatic cascade effects within multi-step pathways. Here, an elegant strategy for studying such behavior, by controlling segregation/combination of enzymes/metabolites in synthetic cell-sized compartments, while preserving vital cellular elements is presented. Therefore, compartments shaped into polymer GUVs are developed, producing via high-precision double-emulsion microfluidics that enable: i) tight control over the absolute and relative enzymatic contents inside the GUVs, reaching nearly 100% encapsulation and co-encapsulation efficiencies, and ii) functional reconstitution of biopores and membrane proteins in the GUVs polymeric membrane, thus supporting in situ reactions. GUVs equipped with biopores/membrane proteins and loaded with one or more enzymes are arranged in a variety of combinations that allow the study of a three-step cascade in multiple topologies. Due to the spatiotemporal control provided, optimum conditions for decreasing the accumulation of inhibitors are unveiled, and benefited from reactive intermediates to maximize the overall cascade efficiency in compartments. The non-system-specific feature of the novel strategy makes this system an ideal candidate for the development of new synthetic routes as well as for screening natural and more complex pathways.

In living cells, there exists an incredible variety of sequential chains of reactions. These so-called reaction pathways are catalyzed by mutually compatible and selective enzymes, which perform central functions, such as breaking down toxins,[1] converting nutrients into energy,[2] or duplicating DNA.[3] To optimize these pathways and thus to guarantee their maximum chance of survival, cells produce enzymes at precise and constant rates.[4] However, because of cellular complexity, determination of optimal enzyme levels is still unclear, in particular because specific enzymatic functions are strongly interconnected with their cascade effects.[5] A smart manner to study the behavior of enzymes, when involved in complex reactions, consists of taking advantage of synthetic micrometer-sized compartments shaped into spherical architectural bodies.[6–8] Though these idealized models favor even partitioning of membrane proteins and simplify diffusion gradients, similarly to cells, they provide the desired membrane selectivity and permeability.[9,10]

Single specific functions have been presented by combining enzymes (the catalytic compounds) with synthetic supramolecular assemblies, either intrinsically semipermeable, such as lipid-coated porous silica particles,[11] protein cages,[12] layer-by-layer capsules,[13–15] and polydopamine capsules,[16,17] or rendered permeable by the insertion of biopores/membrane proteins (acting as "gates" for the passage of molecules), as in lipid-based[7,18,19] or polymer-based[8,20–22] giant unilamellar vesicles (GUVs).

At present, GUVs formed with amphiphilic block copolymers are particularly appealing because they provide enhanced structural membrane properties compared to lipids, since they possess compartments with higher chemical versatility, controlled permeability, robustness, and stability.[23] Nevertheless, common approaches to form polymer GUVs by self-assembly, as electroformation[24] and film-rehydration,[25] rely on the statistical process of encapsulation of biomolecules with a probability of finding the designed amount of one type of enzyme inside the compartments ranging from 12–57%. In the context of elementary biochemical pathways where at least two enzymes are present, this scenario is even more unsatisfactory, with co-encapsulation of two enzymes inside one compartment as low as 10–22%.[26,27] These shortcomings are worsened by the fact that these probabilities have a large uncertainty induced by specific properties of enzymes (e.g., solubility and stability). To date, scientists have struggled to work with state-of-the-art average values for number/mass of enzymes that are vastly non-representative (limited by a small sample size)

Dr. E. C. dos Santos, Dr. A. Belluati, D. Necula, D. Scherrer, C. E. Meyer, R. P. Wehr, Prof. C. G. Palivan, Prof. W. Meier
Department of Chemistry
University of Basel
Mattenstrasse 24a, BPR 1096 4002, Basel, Switzerland
E-mail: cornelia.palivan@unibas.ch; wolfgang.meier@unibas.ch
D. Scherrer, Prof. E. Lörtscher
IBM Research Europe
Saeumerstrasse 4, 8803 Rueschlikon, Switzerland
The ORCID identification number(s) for the author(s) of this article can be found under https://doi.org/10.1002/adma.202004804.

DOI: 10.1002/adma.202004804

and extremely low, due to severe dilution as a result of the self-assembly processes.[28,29]

Double emulsion microfluidics has a significant role to play in the fine control of these parameters (encapsulated content and membrane compositions), coupled with the capability for high-throughput and on-demand generation.[30] However, while double emulsions have been extensively used to form GUVs for programmed release of encapsulated hydrophilic[31–33] and/or hydrophobic[31,34] cargos, their capabilities are still undeveloped for the study of enzymatic pathways, where they are expected to have substantial advantages. In this respect, double emulsions can serve as templates for producing ideal cell-sized compartments with precise control of properties, such as: i) size (as per design) and extremely narrow size distribution; ii) internal biomolecular content and distribution; iii) membrane organization, that is, synthetic membrane composition and insertion of peptides/membrane proteins; and ultimately, iv) features for enzymatic reactions and pathway signaling.

Here, we introduce a novel strategy for studying multi-step enzymatic reactions inside tailored synthetic compartments, systematically arranged in a variety of combinatorial configurations. These compartments in the form of polymer GUVs have been produced via the high precision double emulsion technique, which allows the vital control of the amount/number/ratio of encapsulated enzymes. Moreover the technique has been optimized to render the membrane of the GUVs permeable for diffusion of enzymatic substrates/products in and out of the compartments to support in situ enzymatic reactions. To obtain GUVs with essential properties for insertion of peptides/membrane proteins that make their membranes permeable, we selected amphiphilic block copolymers, based on poly(dimethylsiloxane) (PDMS) and poly(2-methyl-2-oxazoline) (PMOXA) as the corresponding hydrophobic and hydrophilic domains, which have already been used to produce GUVs with the required fluidity and flexibility.[35] Together with the enzymes encapsulated inside the GUVs, equipping GUVs with biopores/membrane proteins allows investigation of multi-step cascade reactions via the spatial segregation/combination of various enzyme types in different compartments. A three-step cascade reaction, based on well-known enzymes, was selected as a model to provide evidence on how the overall reaction can be affected by compartmentalization and single enzyme behavior. A combinatorial strategy based on a plethora of possible segregation configurations, for example, with enzymes separated from one another or in several combinations of encapsulation and co-encapsulation scenarios, was facilitated by the straightforward manner in which double emulsion microfluidics controls the production of the enzyme-loaded GUVs. Thanks to the constant enzyme molar ratios provided by our method, effects, such as the proximity of enzyme and metabolites, and molecular diffusion through membranes have been decoupled, thus allowing limiting factors to be understood and cascades optimized. This fine spatial control provides optimum conditions for reducing competing side reactions, decreasing the accumulation of inhibitory or reactive intermediates, and ultimately increasing reaction rates by maximizing the cascade productivity.

Furthermore, this strategy allows the steps for studying and optimizing complex cascade reactions to be established in a controlled space and time manner, without involving the difficult and time consuming labor of varying enzymatic concentrations. Thus, our combinatorial study represents a system-independent tool for coordinating multi-step pathways, with complexity closer to that of cells for exploring new domains of application.

In the literature, two separate approaches have been used for the creation of double emulsion templated GUVs in microfluidic devices, using glass capillaries or molded in PDMS. Each one has its own advantages and limitations. Glass capillaries have been widely used for production of different types of capsules,[32,36,37] including GUVs with ultra thin shells,[38,39] but the device production and operation are quite challenging: If capillaries are misaligned or not well sanded, instabilities can occur and double emulsions might not be produced because of uncontrolled encounter of the fluids.[40] Reproducible fabrication of microfluidic devices is more easily achieved if they are made from masks and molds, which is predominantly the case when soft lithography is employed to fabricate microchips made from PDMS.[41] However, despite rapid prototyping and easy replication, there are difficulties in modifying the chemical properties of PDMS surfaces to tune their wettability toward different fluids.[38] Forming double emulsions in these conditions requires the oil phase enveloping the inner droplets to be thicker to avoid their collapse, and this may prevent assembly of the GUVs.[42] Thus, to obtain GUVs with a homogeneous polymeric membrane that favors biopore/membrane protein insertion, a higher level of precision and reproducibility is required for generating double emulsions with thin organic shells, which neither glass capillaries nor PDMS microdevices alone can in the long run provide. For this reason, we now combine the best characteristics of both aforementioned approaches to produce novel microfluidic devices that are based on high-resolution solid-state manufacturing and aim at exploiting the high chemical and mechanical compatibility of silicon-glass devices. For that purpose, channels were etched into a silicon (Si) substrate using deep-reactive ion etching (DRIE) (that provides rectangular cross-sections with a desired depth, described in Supporting Information), and were closed with glass covers by anodically bonding them to the Si substrate. Both the native oxide of the Si bottom channel walls as well as the glass channel top wall offer universal solvent compatibility (avoiding channel swelling) and multiple ways to control surface chemistry. Furthermore, the architecture provides a high mechanical robustness, in particular compared to PDMS-based devices, which prevents oscillatory "breathing" of the channels upon operation, preserving the geometry of the junction, important for double-emulsion generation.[43]

While the initial design of our microchips was based on an existing six-way junction,[44] several improvements in the geometry were necessary for optimal double emulsion formation and flow to collection (Figure S1, Supporting Information). To create double emulsions, the silicon-glass channels were functionalized to locally control the wettability within regions of the microchip, where channel properties were made hydrophilic or hydrophobic (Figure S2, Supporting Information).

Polymer stabilized water-oil-water double emulsions were generated by feeding immiscible fluids with defined flow rates into the six-way junction (**Figure 1**). In such a geometry,

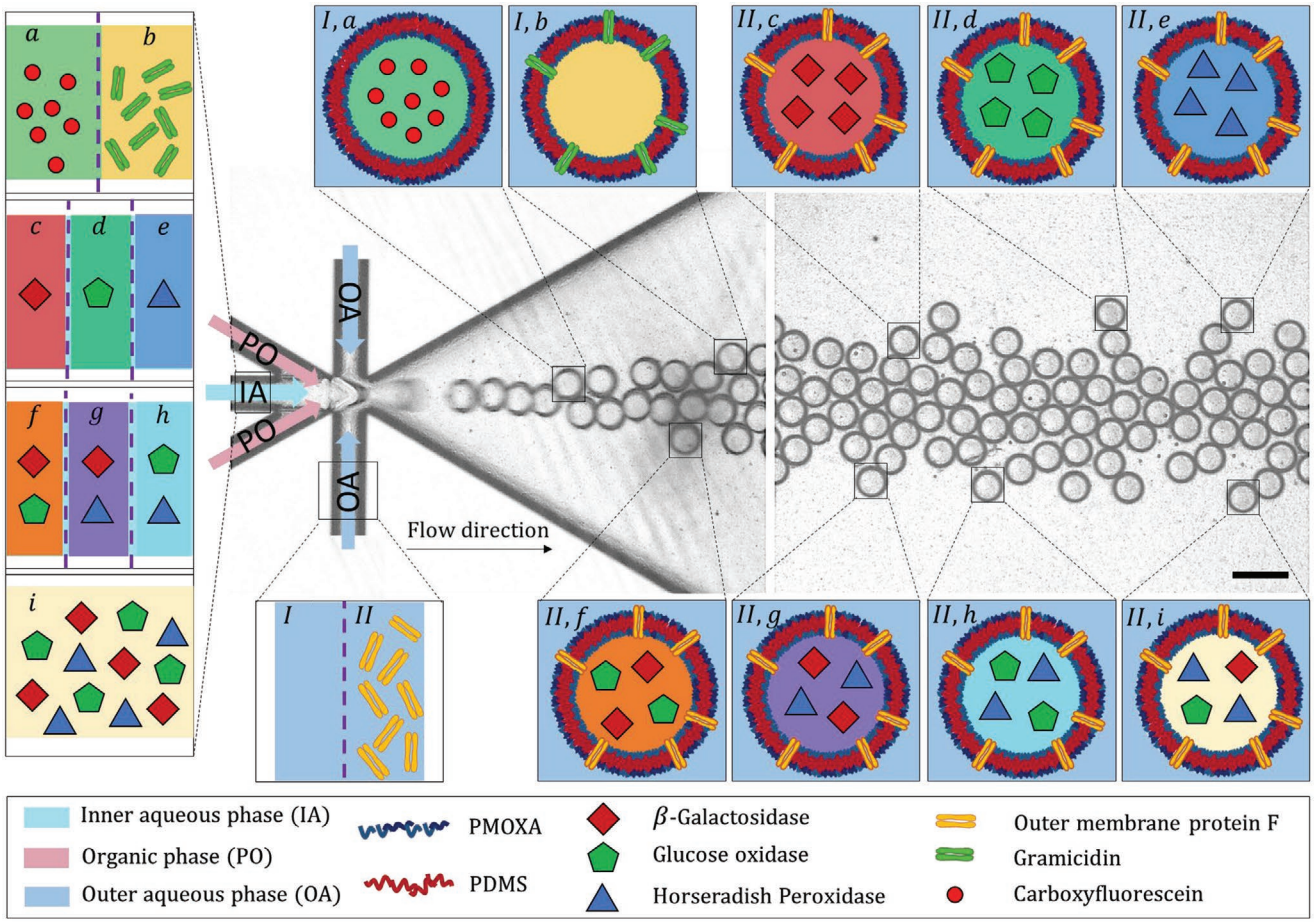

Figure 1. Microfluidic process of simultaneous double emulsion generation and functionalization. Schematic representation of the high-throughput double emulsion generation process for creating compartments (giant unilamellar vesicles, GUVs, [Movie S1, Supporting Information]) containing precise amounts of biomolecules in a plethora of possible combinations in their inner aqueous cavity and inside their polymer membrane. a–i) Representation of the various inner aqueous (IA) biomolecular content. I,II) Representation of the different outer aqueous (OA) phases. Schematic: I,a) Impermeable GUVs loaded with aqueous solution of carboxyfluorescein, and I,b) GUVs equipped with the biopore gramicidin. Schematic of GUVs equipped with the outer membrane protein, OmpF, and loaded with aqueous solutions of enzymes, β-galactosidase, glucose oxidase, and horseradish peroxidase, encapsulated/co-encapsulated as: II,c–e) singlets (one enzyme); II,f–h) duplets (two enzymes); and II,i) triplets (three enzymes). Scale bar: 100 µm.

resulting from the combination of co-flowing and flow-focusing junctions, the inner aqueous (IA) phase stream enclosed by the polymer organic (PO) phase (due to its affinity toward the channel wall) advances downstream from the hydrophobic side to the hydrophilic main channel, up to the point, where surface forces no longer hold the shear provoked by the outer aqueous (OA) phase (which preferentially wets these channels), and the break-up occurs. In coaxial glass capillaries[37,45] and in planar devices,[46] where either co-flowing or two serial flow-focusing junctions were used, dripping instabilities only allowed for pinching the inner drop before the outer jet, and a mixture of single and double emulsion droplets were mainly produced.[40] However, our six-way junction not only provided monodispersed double emulsions with the desired thin shells at 100% production efficiency (after optimization of flow rates), but also at high OA phase flow rates (50–80 µL min^{-1}) providing a simultaneous high-throughput break-up of both fluids (IA and PO) in a single step (Movie S1, Supporting Information).

The excellent ability to control size and composition that our microfluidic devices offer should allow GUVs to be equipped not only with small biomolecules, such as carboxyfluorescein, but also larger ones, such as proteins, both in the inner cavity and inside the polymer membranes (Figure 1). Their modularity yielded a variety of GUV arrangements that allow the study of enzymatic cascade reactions. For constructing robust, and at the same time flexible, cell-sized compartments for assisting insertion of biochannels,[23] the amphiphilic diblock copolymer poly(dimethylsiloxane)-*block*-poly(2-methyl-2-oxazoline) ($PDMS_{26}$-*b*-$PMOXA_9$) was synthesized and purified according to previously reported protocols.[47,48] The copolymer was added to the PO phase, first to stabilize the double emulsion, and subsequently, to form the supramolecular membrane of the GUV. In principle, our microfluidic platform could also produce lipid-GUVs, since this has been already done, both in glass capillary devices,[38] as well as in PDMS chips.[44] In that case, a lipid-carrying organic phase would be fed at the PO phase channel, instead

of the selected copolymer. However, this is out of the scope of the current work.

In addition, we aimed to mimic elements of the complex interiors of cells, by loading precise amounts of enzymes into GUVs. Hence, one, two, or three types of enzymes were added to the IA phase in predefined amounts, either one at a time, in pairs, or all at once. For triggering the cascade reaction, and in general for providing communication between the constructed compartments, either a pore-forming peptide was added to the IA phase, or a membrane protein was added to the OA phase (Figure 1). Both strategies for double emulsion formation enabled a controlled reconstitution of the biochannels (each offering a specific molecular flow), in a reproducible manner during the process of reorganization of the polymeric chains into the GUV membrane.

Polymer GUVs formed using double emulsions as templates do not rely on the self-assembly of amphiphiles in bulk.[40] Instead, these amphiphiles self-assemble at the two liquid liquid interfaces of the double emulsions and form two monolayers, which are brought together during solvent evaporation, and finally shape into a membrane bilayer. As a result of the thin shell of the produced double emulsions, such a transition occurred within minutes and resulted in GUVs with a homogeneous membrane composition that is ideal for inserting biochannels.

Droplets produced by dripping, in which their pinch off occurs near the tip before entering the main channel, are typically highly monodispersed,[45] but strongly dependent on parameters, such as the capillary number, Ca ($Ca = \mu v/\gamma$, where the numerator accounts for the viscous shear stress and the denominator for the interfacial forces[49]), the viscosity ratio, and the junction geometry. Understanding how these parameters influence the double emulsion formation, and ultimately the GUV size and size distribution, is of fundamental importance to achieving the thin shell thickness and desired regularity of GUVs. Since the flow dynamics underlying the break-up mechanism of double emulsions is rather difficult to simulate and predict, scaling laws for GUV sizes are not established.[50,51] Hence, we perform empirical optimization for conditions where double emulsions were in flow to examine the influence of, first, the outer aqueous (OA) flow rate on the droplet break-up, and second, the inner aqueous (IA) flow rate on the double emulsion organic shell thickness. The outer and the inner diameter of the double emulsions (**Figure 2**a) were measured using an automated image processing software written in Matlab (Supporting Information) to enable statistically relevant numbers of GUVs to be analyzed. For a specific example, 2361 droplets were measured and found to have size distributions with mean diameter of the inner, $\overline{D}_{\text{in}}$, and the outer shell, $\overline{D}_{\text{out}}$, of 35.54 and 47.80 μm, respectively, and very narrow polydispersities (i.e., relative standard deviations, $\sigma_D/\overline{D}$) of around 1.70% (Figure 2b). This same procedure was applied to obtain mean diameters and polydispersities of all double emulsion populations generated, so that their size homogeneity could be guaranteed.

First, the flow rate ratio of the inner aqueous phase to the polymer organic phase was set to an intermediate and fixed value, that is, $Q_{IA}/Q_{PO} = 2$, whereas the outer aqueous phase flow rate, Q_{OA}, was varied between 10 and 80 μL min^{-1}, covering about an order of magnitude of Ca numbers. Both inner and outer diameters decreased when Q_{OA} was increased, but reached a plateau after a certain value (Figure 2c). When this threshold was exceeded (for $Q_{OA} > 40$ μL min^{-1}), the influence of the junction geometry on the double emulsion size prevailed over the viscous shear stresses. Consequently, if necessary, double emulsion mean sizes can be reduced by decreasing the junction dimensions accordingly; smaller channels can be easily etched in the silicon substrate (with micrometer precision[52]). It is interesting that the same general behavior was not only already reported for similar geometries producing double emulsions,[32,53] but also for simple T-junctions operating at much lower capillary numbers.[54,55] This suggests that despite their apparent complexity, at the dripping regime double emulsions follow the same rules of formation as single droplets, as long as the inner droplet is stable inside the envelope of the organic phase. Second, the OA phase flow rate was set to a constant value above the threshold, that is, $Q_{OA} = 50$ μL min^{-1}, and the flow rate ratio Q_{IA}/Q_{PO} was varied. For values below 1, single oil droplets break up in between double emulsions, whereas for values larger than 2.5, surface forces on the oil side do not hold and the droplet blows up before the junction; both are undesirable situations (hence not shown). Sizes of the double emulsions were nearly independent for Q_{IA}/Q_{PO} between 1–2.5 (Figure 2d). On one hand, this implies we can profit from the versatility of the system and operate anywhere in this window, but on the other hand, we have no means of reducing further the organic phase shell thickness. Note that this behavior is only valid if Q_{OA} is sufficiently high and above the threshold mentioned above (Figure 2c,d). Overall, by using the six-way junction geometry together with specific flow rates and flow rate ratios among the fluid phases, we have successfully generated double emulsions that were surrounded by a thin organic shell.

Finally, to obtain GUVs from double emulsion templates, the middle organic phase has to partition out of the droplet, the so called "dewetting".[38,56] This is a complex process, which depends, among other things, on solute–solvent attractions (solubility), solvent vapor pressure, and on the attractive forces between the molecules at the fluid interfaces. A correct balance of such energies would result in a complete dewetting.[57] However, despite efforts and claims of "solvent-free" GUV formation,[44,57,58] from the best of our knowledge, as of today, there exists no work that could eliminate the possibility of remaining solvent traces in the membrane bilayer. Similarly, in our system, the dewetting process occurred very fast (it could not be measured) up to a certain extent; that is, it reached an equilibrium state, which consisted of having a small, but visible oil/polymer pocket on the GUV surface that stayed there even after days (inset in Figure 2e). For estimating size and size distribution, the resulting GUVs were imaged by confocal laser-scanning microscopy (CLSM) (Figure 2e). Diameters were obtained by treating the acquired microscopy images with the same image processing software as that used to measure the diameter of the double emulsions. As a result of the precise control of double emulsion sizes (D_{in} and D_{out}), GUVs have similar very narrow size distributions (Figure 2f), with diameters of 38.14 ± 1.4 μm (± 3.7%). This is in contrast to polymer GUVs formed by direct self-assembly in dilute

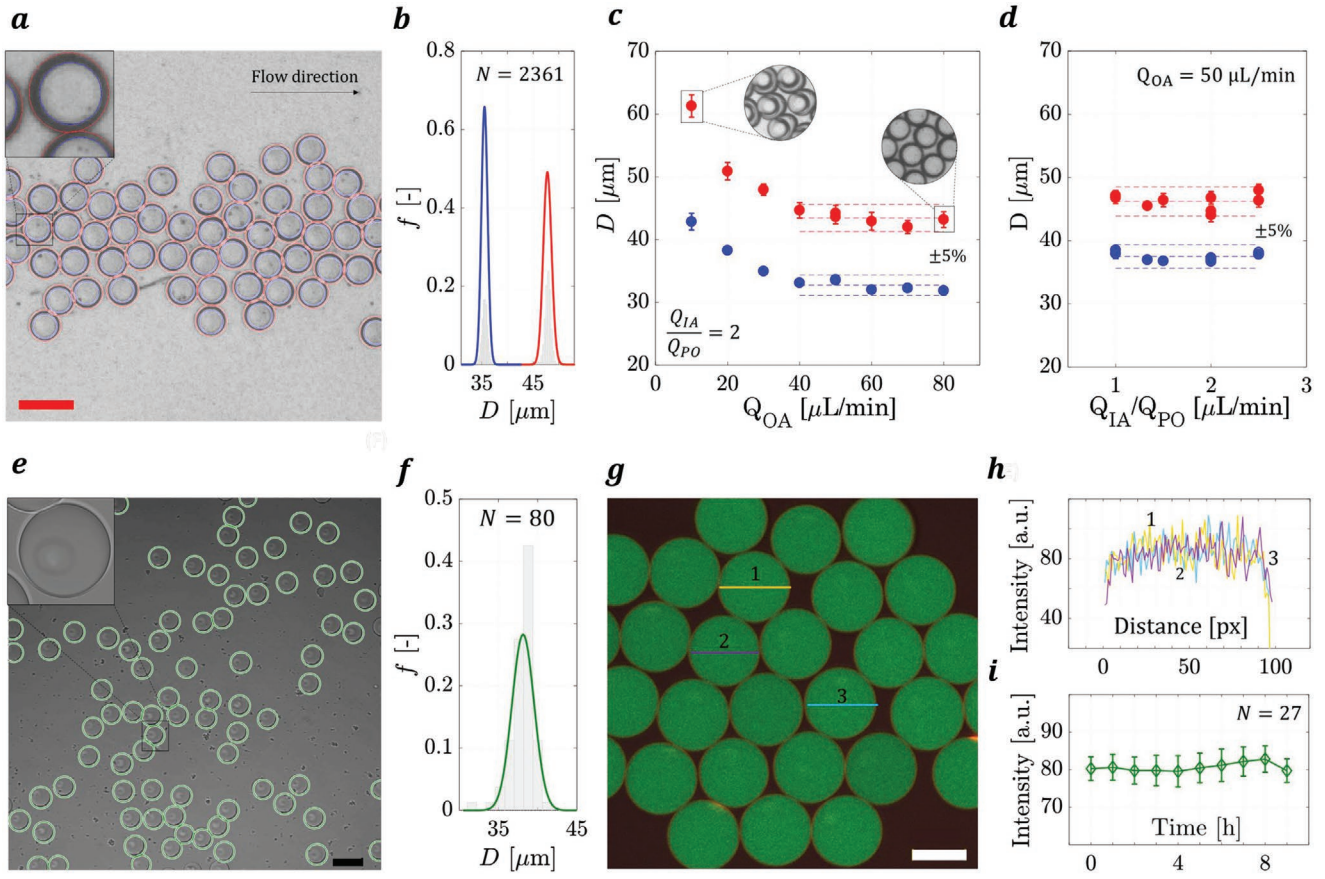

Figure 2. Optimization of double emulsion sizes and characterization of sizes and permeability of GUVs. a) Representative image of double emulsions flowing in the main channel of the microfluidic chip; the outer diameters (red circles) and the inner diameters (blue circles) of the double emulsions were measured using image processing software written in Matlab; scale bar 100 μm; inset: visualization of how well features of outer and inner diameter were captured by the software. b) Histograms and their corresponding regressed normal distributions out of 2361 measured droplets; mean diameter of the inner droplet, $\bar{D}_{in}$ = 35.54 μm and the outer shell diameter, $\bar{D}_{out}$ = 47.80 μm. Both size distributions resulted in polydispersities (i.e., relative standard deviations, $\sigma_D/\bar{D}$) of around 1.70%. c) Inner and outer diameter variation as a function of the outer phase flow rate, Q_{OA}, at a fixed flow rate ratio, Q_{IA}/Q_{PO} = 2. d) Inner and outer diameter variation as a function of the flow rate ratio, Q_{IA}/Q_{PO}, at a constant outer phase flow rate Q_{OA} = 50 μL min^{-1}. Error-bars are given by the standard deviation. The dashed lines represent ±5% deviation from the mean diameter (center line). e) Exemplary CSLM image of the resulting polymer GUVs; scale bar: 50 μm. The diameters of the GUVs (green circles) were measured using the same software as (a); inset: zoom-in of a GUV containing a pocket on its upper surface. f) Histogram and its regressed normal distribution out of 80 measured GUVs; mean diameter, $\bar{D}$ = 38.14 μm and $\sigma_D/\bar{D}$ = 3.7%. g) CLSM image of GUVs loaded with carboxyfluorescein at the beginning of the permeability experiment (t = 0); scale bar 20 μm. h) Fluorescence signal intensity measured along the centerline of three representative GUVs. i) Fluorescence intensity change over time.

solutions, which had a larger size distribution, in the range between 2 to 40 μm.[28,59]

Additionally, as the amphiphilic diblock copolymer $PDMS_{26}$-*b*-$PMOXA_9$ was employed for assembly of the compartments, we expect the GUVs to be impermeable to small molecules.[24,28] Nonetheless, since the method of GUV formation influences the mode of self-assembly, it might also induce changes in the membrane permeability. To ensure that GUVs are impermeable, a fluorescent dye, carboxyfluorescein (CF, 376 Da) was loaded into GUVs as representative of the molecular weight of several molecules of biological interest, such as disaccharides or nucleotides,[60] and the change in fluorescence intensity inside the core of the GUVs was followed over a period of 9 h at 1 h intervals (Figure 2g–i). The minimal signal change (within the deviation) indicated that in spite of the existence of a small oil pocket, GUVs were impermeable. Being able to preserve this characteristic is important for triggering permeability in a controlled fashion.

Inspired by the self-regulation of activity and signaling pathways enabled by cell membranes, we explored functionalities which favor inward and outward flow of selected ions and molecules by equipping membranes of GUVs with channels that enable in situ reactions.[24,27,28,61] For screening possible functionalities, we selected two different well-known and stable biomolecules,[62–64] a polypeptide and a transmembrane protein, which differ greatly in size, shape, and transport specificity, thus having different effects on membrane permeability.[8,24] When peptides/membrane proteins are reconstituted into the GUVs membrane, its thickness is irrelevant; the pores will allow the selected ion/molecule to flow inward and will trigger the specific process, if they preserve their functionality. On the contrary, channel sizes are always associated to the particular

enzymatic reaction; hence, depending on them, molecules of lower or higher molecular mass will be allowed to cross the membrane. Exactly as in nature, each membrane has a specific cutoff and functionality.[4,28]

The insertion of membrane proteins inside synthetic membranes relies on membrane properties such as thickness, surface roughness, and curvature.[65] These dependencies make insertion and chemical integrity preservation of the biomolecule a difficult task, particularly in polymeric membranes.[62] However, despite the much ticker membrane of polymersomes, the high flexibility of PDMS provides membrane fluidities allowing successful insertion of membrane proteins that must overcome the significant higher hydrophobic mismatch between their size and the membrane thickness; this is a key-factor for membrane proteins incorporation.[7,9]

First, specific permeability of GUV membranes was probed by inserting a biopore, the pore-forming peptide gramicidin (gA), which allows controlled passage of protons and other monovalent cations.[24] Then, we aimed to equip the GUV membranes with protein channels that induce permeability of enzymatic substrates/products, and selected the bacterial outer membrane protein F (OmpF), which enables a size selective molecular flow up to 600 Da.[8,62,64]

Both OmpF and gA have already been inserted in synthetic membranes based on PDMS and PMOXA copolymers,[9,29,35] but whereas OmpF was reported to be functional inside membranes affording a significant mismatch (up to 6 times) between its pore length and the membrane thickness of the polymer GUVs, gA preserved functionality only in membranes with a maximum thickness of 12.1 nm, resulting in a mismatch of approximately 4.5 times.[24] Thus, the $PDMS_{26}$-*b*-$PMOXA_9$ diblock copolymer used in this study, with an estimated thickness of 12.6 ± 1.3 nm (Supporting Information), was carefully selected so as not to exceed significantly the literature threshold for the biopore/membrane protein insertion. Since control of the amounts of biomolecules that can be loaded into GUVs formed via double emulsions is the most important advantage of this technique, peptides and membrane proteins were introduced into the system (one at a time) during the generation of double emulsions in the microfluidic device (Figure 1). Gramicidin added to the IA phase for forming the inner droplet, enveloped by the organic phase, was the best strategy to present the largest surface, which thus favors diffusion and final reconstitution of the biopore in the membrane. To assess the biomolecular interactions via CLSM, gA was co-entrapped with a hydrophilic dye, Sodium Green (SG), which emits fluorescence in the presence of Na^+ ions. The increase in fluorescence inside GUVs, associated with the inflow of Na^+ after addition of an external NaCl solution, indicated successful gA insertion in the synthetic membrane (**Figure 3**a) (Movie S2, Supporting Information), even though the latter is roughly 4.8 times thicker than the gA pore length.[24] Further control experiments can be found in Figure S6, Supporting Information.

OmpF was added to the OA phase. At high Q_{OA} (still at the laminar regime), OmpF aggregates flowed downward, together with the polymer stabilized double emulsions in the main channel, and controlled close contact was promoted between OmpF and the polymer molecules, so as to facilitate its penetration. This new mechanism follows a strategy known to assist efficient membrane protein recruitment, as to profit from the

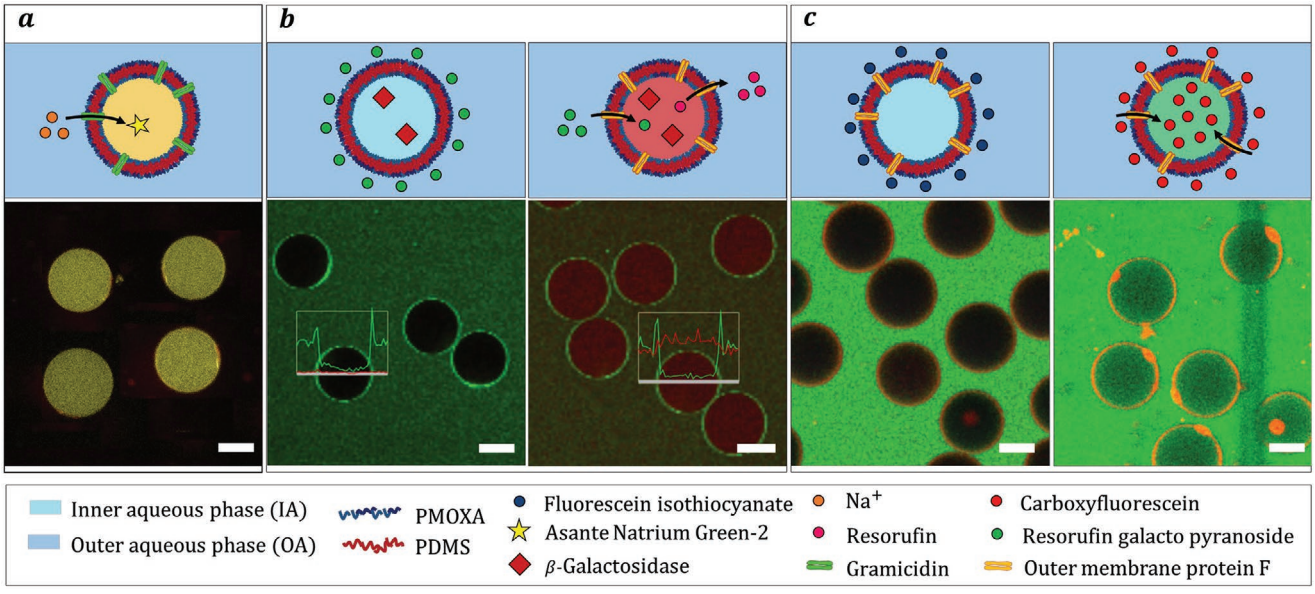

Figure 3. GUVs equipped with biopores and membrane proteins. According to the corresponding top schematics, CLSM images show: a) GUVs equipped with biopore gramicidin (gA), containing sodium Green (SG), which increased fluorescence after the passage of Na^+ ions through the gA formed pore. b) On the left-hand-side (l.h.s), GUVs containing the enzyme *β*-galactosidase (*β*-gal), in the absence of the pore-forming outer membrane protein F (OmpF), did not allow the substrate resorufin galacto pyranosidase (RGP) to penetrate the polymer membrane; the red fluorescence signal is flat (inset). On the right-hand-side (r.h.s), GUVs containing *β*-gal and equipped with OmpF allowed RGP to penetrate the polymer membrane and react, yielding the fluorescence product resorufin; the red fluorescence signal is high inside the GUV (area of production) and lower outside, after product outflow (inset). c) Size selectivity. On the l.h.s, GUVs equipped with OmpF restricted the passage of the fluorescein isothiocyanate dextran (FITC-dextran, 10 kDa). On the r.h.s, GUVs equipped with OmpF allowed the passage of carboxyfluorescein (CF, 376 Da). Scale bar: 20 μm.

low membrane stability at the early stage of its formation process.[65] In addition, during the dewetting, as the two leaflets of the bilayer approach, the osmotic imbalance causes the inner core to shrink as water leaves, unless OmpF insertion happens and the new pore helps to equalize the osmotic pressure. Thus, the higher osmolarity of the collection phase (CP) might also have played a role in destabilizing the membrane and aided full transmembrane protein insertion during reorganization of the polymeric chains in the GUVs membrane.[66,67]

Therefore, to assess the functionality of OmpF insertion, GUVs with and without inserted OmpF, which contained the enzyme β-Galactosidase (β-gal), were exposed to the enzymatic substrate, resorufin galacto pyranoside (RGP), and the change in fluorescence intensity along the GUV centerlines was detected in the acquired CLSM images (exemplary signal variations are shown in the insets of Figure 3b). These indicate that when OmpF was present, RGP diffused inside the GUV lumen, resulting in a fast production of resorufin (Figure 3b), while in the absence of OmpF, no fluorescence signal associated with resorufin was detected. In addition, the OmpF functionality was further explored for inward diffusion of molecules smaller than the OmpF cutoff. Diffusion of the dye carboxyfluorescein, which is smaller than 600 Da, through the GUV membrane was detected after 24 h in the acquired microscopy images (Figure 3c) by an increase of the fluorescence intensity of about 150% (Figure S7, Supporting Information). As expected, larger molecules, such as fluorescein isothiocyanate dextran (FITC-dextran, 10 kDa), did not penetrate, as only a minor change in signal intensity was observed (which after a *t*-test was shown to be insignificant at a significance level, $p < 0.05$) (Figure S7, Supporting Information). The results, and particularly our controls, support the impermeability findings and also highlight the lack of defects (no leakage) of the polymeric GUV membranes, which represents an important advantage over lipidic GUVs.

OmpF was also added to the IA phase when forming the double emulsions, and following the same reasoning as for gA, it was expected that confinement would result in the maximum surface contact for OmpF insertion. However, since the OmpF solution was fed at low flow rates and in the form of a slurry of aggregates, because of the absence detergent (necessary to keep OmpF solubilized), it entered the microchip channel intermittently, which hampered its final membrane penetration. Thus, incorporation of OmpF in the polymeric membrane was more successfully performed when it was added to the OA phase (Figure S7, Supporting Information).

Lastly, as both OmpF and gA have no directional flux, all biopores incorporated in the membrane of the GUVs are functional and serve for molecular flow-through. Thus, with a rough estimation (Supporting Information), we obtained a total amount of 1×10^6 molecules of OmpF and of 3×10^6 molecules of gA per GUV, which corresponds to 254 OmpF μm^{-2} and 710 gA μm^{-2}. Overall, when equipped with biopores/membrane proteins, GUVs formed by $PDMS_{26}$-*b*-$PMOXA_9$ fulfill the complex requirements of permitting molecular flow, and mimicking various conditions for cell communication, ranging from unselective permeability of molecules with limited weights to very precise reactions, in which bio-specificity is needed.

Certain fundamental similarities are shared between different cell types. Specifically, they contain the same proportion of enzymes within cells, which coordinate biochemical reactions.[4] Thus, providing conditions in which the relative amounts of enzymes are tightly controlled is vital for mimicking complex cell environments for optimizing biochemical pathways. Forming GUVs via the double emulsion microfluidics overcomes the issues caused by stochastic encapsulation of the self-assemblies, such as low and distributed concentrations of enzymes.[62] To date, double-emulsion templated polymer GUVs have primarily been employed in cargo delivery, where maintaining the inner concentration constant was probably not crucial, since it was rarely quantified.[31,56,68] To conduct multi-step cascade reactions inside compartments, keeping the stoichiometry between enzyme concentrations is of extremely importance. Thus, to quantify the concentration of encapsulated enzymes (**Figure 4**a–f), encapsulation and co-encapsulation efficiencies of fluorescence-labeled enzymes were estimated inside GUVs (with negligible change in size due to difference in osmolarity of the phases) by brightness measurements associated with fluorescence correlation spectroscopy (FCS) (Experimental Section). Thus, brightness measurements were conducted for two model enzymes, β-galactosidase (β-gal) conjugated with Cy5 and glucose oxidase (GOx) conjugated with OregonGreen in the cases where each enzyme type was individually loaded (Figure 4a, β-gal and b, GOx, respectively), and in the case where the two types were loaded together in the same GUV (Figure 4d). However, horseradish peroxidase (HRP) conjugated with Atto 550 associated with the membrane because of its hydrophobic properties, thus preventing its measurement (Figure 4c).

The encapsulation efficiency, EE, was calculated as $EE = c_e/c_0 \times 100\%$, where c_0 is the measured concentration of a single enzyme in the solution used to prepare the GUVs (inner aqueous (IA) composition, Experimental Section), and c_e is the measured concentration of the same enzyme inside the GUV. Similarly, co-encapsulation, cEE, was calculated as, $cEE = 2c_e/c_0 \times 100\%$; this quantity was multiplied by two, since the two enzyme types with their respective c_0 were added together in a 1:1 mass ratio when forming the GUVs. Encapsulation and co-encapsulation efficiencies reached nearly 100% within the experimental statistical resolution, indicating that the double emulsion technique provides great control of the biological content inside the GUV and a very high encapsulation efficiency is achieved (**Table 1**). This feature is key and makes our platform great for screening/studying/optimizing multi-steps cascade reactions.

Overall, we show that microfluidics can not only allow precise amounts of enzymes and stoichiometric ratios of different types of enzymes to be placed inside compartments, but also allow the production of large populations of GUVs with uniformly distributed concentrations. Hence, for the first time, high concentrations of encapsulated enzymes could be achieved almost deterministically and in a controlled manner inside GUVs, which compensate the limiting diffusion distances,[3,69] and support the optimization of biochemical pathways.

To study multi-enzymatic pathways, we take advantage of the capabilities of our microfluidic method to construct synthetic compartments with guaranteed absolute and relative enzymatic quantities, which are spatially segregated/combined in different GUVs to produce well-defined conditions for activating

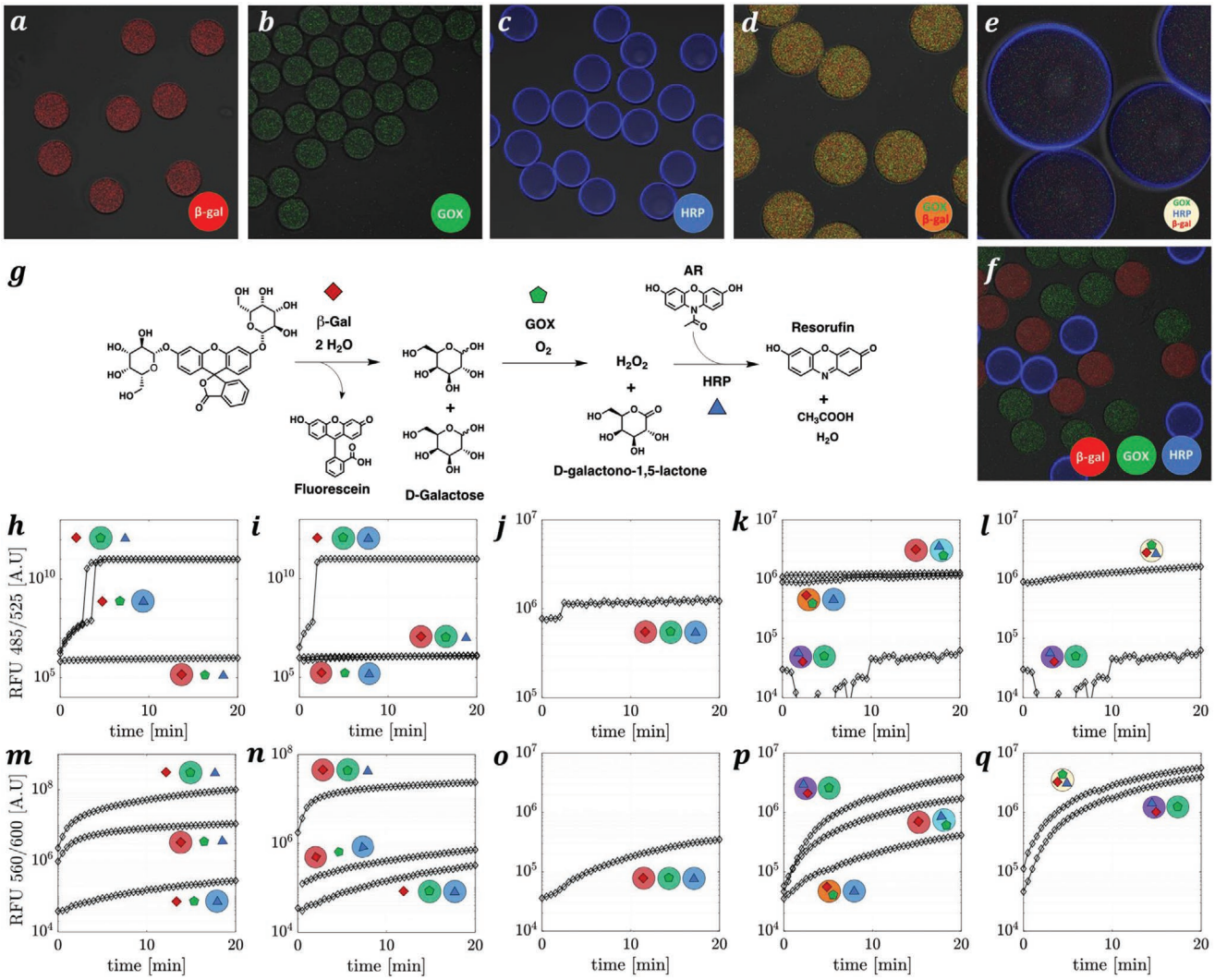

Figure 4. Combinatorial study of a three-step cascade. Representative CLSM images of GUVs containing: a) only β-gal enzymes labeled with Cy5; b) only GOx enzymes labeled with Oregon green 488; c) only HRP enzymes labeled with Atto 550. Scale bar: 50 µm. d) Both GOx and β-gal in a (43:139) molar proportion. Scale bar: 20 µm. e) All three enzymes, β-gal, GOx, and HRP in a (43:139:1) molar proportion. Scale bar: 10 µm. f) Either β-gal or GOx or HRP segregated. Scale bar: 50 µm. g) Scheme of the three-step cascade reaction. Representation of enzymes: ◊ for β-gal; ⬠ for GOx; and △ for HRP. Change in fluorescence intensity over time of the products: h–l) fluorescein (485/525 nm); m–q) resorufin (560/600 nm).

biochemical pathways. The effect of confinement on cascade reactions has already been characterized in a binary system inside smaller polymersomes produced via self-assembly, where the enzymatic efficiency was enhanced by the reduced volume of the compartment.[25] By using double-emulsion microfluidics, high enzymatic concentrations can easily be achieved, which consequently increases reaction efficiency, independently of the size of the GUV. Moreover, more complex enzymatic cascades in synthetic compartments approach the complexity of real cells, and the role that compartmentalization plays on the outcome of intermediate and final products has previously not been investigated.[70] In order to demonstrate this, we

Table 1. Efficiency of encapsulation, EE, and co-encapsulation, cEE, of fluorescence-labeled enzymes (β-gal and GOx) individually loaded in different GUVs and loaded together in the same GUV.

	β-gal	β-gal and GOx	GOx	GOx and β-gal
	(at 655 nm)	(at 655 nm)	(at 488 nm)	(at 488 nm)
Concentration of enzymes in IA, c_0 (mg mL^{-1})	0.235 ± 0.010	–	0.385 ± 0.010	–
Concentration of enzymes in GUVs, c_e (mg mL^{-1})	0.227 ± 0.020	0.109 ± 0.010	0.375 ± 0.030	0.208 ± 0.010
EE/*cEE* (%)	96.6 ± 9.8	92.8 ± 7.6	97.4 ± 11.0	108.0 ± 9.2

selected a three-enzyme cascade reaction model, which allowed the investigation of how reactions can be affected by segregation of enzymes inside different spatial organization of GUVs. The particular model may be seen as mimicking the pathway for the digestion of β galactosides, which plays an important role, yet specific for some cells. For instance, in organisms, the enzymes can also hydrolyze lactose into galactose and glucose, which will further proceed into glycolysis.[71] Thus, the proposed model was based on the following three enzymes: β-gal, GOx, and HRP. The first enzyme, β-gal, hydrolyses fluorescein-di-β-galactopyranoside (FGP) into fluorescein and galactose; in the absence of glucose, GOx can oxidize galactose and produce hydrogen peroxide (H_2O_2),[72] which is used by HRP to oxidize Amplex Red (AR) into resorufin. This cascade performed by well-known enzymes allows accurate identification of which phenomena are due to diffusion;[73–75] additionally, the choice of FGP instead of the canonical lactose allows two reactions to be followed fluorometrically, and to infer the behavior of the middle one that does not produce fluorescent species, thus providing a deeper insight as to how enzyme activities were affected by the three-step cascade in confined spaces. Moreover, we kept the focus on maintaining the relative enzymatic concentrations constant for highlighting the versatility of our system in providing the many possible physical segregation and combinations for studying a multi-step cascade reaction.

Segregating enzymes in independent compartments organized in different arrangements induces a complex scenario at the molecular level because it affects: i) the passage of molecules across semi-permeable membranes (which might be reduced due to the pore size), ii creation of non-homogeneous concentrations of enzymes, iii) subsequent reactions from the cascade that are influenced by the dilution effect, which occurs when molecules leave the compartment and enter the bulk environment, and iv the probability that molecules enter in the "right" GUV (i.e., that substrates meet the correct enzyme, which would allow the sequence of the cascade to operate), which decreases with the degree of segregation. These effects are thus defined by the cascade topology; in short, where each enzymatic reaction takes place relative to each another, and to how many membrane passages and dilution steps the substrates and products are subjected.

As a result of constant enzyme molar ratios (β-gal : GOx : HRP, 43 : 139 : 1), we could study variations of enzyme segregation, with enzymes separated from one another and in several combinations of encapsulation and co-encapsulation (e.g., three enzymes encapsulated together, separated in three different GUVs, or only two encapsulated and a third in the bulk). In such situations, difference in compartmentalization arrangements is the only dependent variable.

Initially, we studied the cascade in the simplest topology, namely encapsulating just one enzyme at the time inside GUVs. To conduct the cascade, the complementary enzymes were placed in the surroundings, which caused instantaneous consumption of the available substrate, and made possible to elucidate the effects of molecular passage through OmpF pores inserted in the GUV membrane. The production of fluorescein (product of the first step of the cascade reaction) depends only on the availability of the substrate FGP to β-gal, and the reaction is slowed directly when this enzyme is encapsulated (Figure 4h). On the contrary, the production of resorufin (the final product of the cascade reaction) is affected by the whole cascade, especially the availability of substrates, H_2O_2 (dependent indirectly on galactose) and Amplex Red to HRP; when this enzyme is encapsulated, the overall cascade is likewise slowed, once again due to diffusion of HRP substrates through the membrane. However, by analyzing the configuration where GOx is encapsulated, we obtained the highest production of resorufin. As the diffusion of H_2O_2 to the surroundings is fast, we were able to decouple the effects and observed that the rate determining step is the slow diffusion of Amplex Red into the HRP-loaded GUV, in agreement with the literature.[25] In the case of GOx-loaded GUV arrangements, external AP is readily available to HRP (Figure 4i).

In arrangements where two enzymes were individually encapsulated in different GUVs and the third enzyme was free, a somewhat higher degree of segregation was introduced, and led to more membrane passages and a lower probability that the substrate entered the correct compartment. Mostly, similar trends were observed as for single enzyme encapsulation, that is, unfavored production of fluorescein and resorufin whenever β-gal and HRP were respectively encapsulated (Figure 4j,k). Nevertheless, insights into the diffusion of intermediates were gained by comparing both arrangements in which HRP was encapsulated. In such cases, when, for example, GOx instead of β-gal was confined, the diffusion of galactose (produced by β-gal) across the membrane of GOx-loaded GUVs slowed the process in comparison to GOx free in the surroundings (Figure 4k).

Full segregation of enzymes (i.e., the arrangement where each enzyme is located in a different compartment) contributed significantly to a reduction in production of both fluorescein and resorufin, as expected (Figure 4l,m) (Movie S3, Supporting Information). This outcome is due to several effects: not only must the fluorogenic substrates FGP and Amplex Red cross the membrane inward, but also the so called "bridging molecules," galactose and H_2O_2, which diffuse out of the GUV where they are produced, must enter in the next GUV to reach the enzyme for subsequent reaction. Moreover, with such a degree of segregation (three types of compartment), all involved molecules have a 66% chance of diffusing into a wrong GUV, which further hampers the reaction velocity.

Since we used well-known enzymes, incompatibility issues were not expected.[76] However, additional interesting behavior of the cascade reaction have been revealed by the possibility of positioning enzymes in additional compartmental arrangements based on co-encapsulation of enzymes in one type of GUV.

By using a complex setup, in which enzyme couples were co-encapsulated, we observed that in the arrangement where β-gal and GOx were loaded inside the same GUV (orange circle in Figure 4n,o) and HRP inside another one, represented by (β-gal+GOx)+(HRP) (Movie S4, Supporting Information), the amount of resorufin produced was curiously lower than in the alternative arrangement, in which β-gal was alone in one GUV and GOx and HRP were encapsulated together in a second, (β-gal)+(GOx+HRP) (cyan circle in Figure 4n,o). This seems to contradict fast diffusion of H_2O_2, but what actually happens is that GOx is competitively inhibited by the excess of H_2O_2,[77]

which due to the distance introduced by the compartmentalization, cannot be as rapidly consumed and a harmful environment develops. Moreover, we also consider the possibility that H_2O_2 may have originated from a second oxidation of the highly concentrated metabolite D-galacto-1,5-lactone, thus aggravating the suppression of GOx activity, as the D-galacto-1,5-lactone derived from D-glucose is also a substrate for GOx.[78] Nevertheless, due to the proximity of enzymes offered by co-encapsulation in the arrangement (β-gal)+(GOx+HRP), HRP accesses H_2O_2 immediately and converts it into resorufin. An interesting situation happened in the arrangement where β-gal and HRP were located inside the same GUV (purple circle in Figure 4n,o) and GOx inside another one, represented by (β-gal+HRP)+(GOx). In this arrangement, both bridging molecules (galactose and H_2O_2) should travel between GUVs, a topologically similar situation to all enzymes segregated), which, as already discussed, would decrease the resorufin production rate. However, the result is quite the opposite, and much larger production of resorufin was coupled to almost no fluorescein signal. This behavior rises because HRP, besides oxidizing H_2O_2, can also oxidize the fluorescein released by hydrolysis of FGP into non-fluorescent compounds;[79] this reaction is favored because H_2O_2 is produced in the other GOx-loaded GUV, which hampers its access to HRP. Furthermore, decomposition of fluorescein produces the radical hydroxyl ($\cdot$OH), which is a potent and non-specific oxidizing agent. Amplex Red was thus oxidized both by the combination HRP + H_2O_2 and by $\cdot$OH, leading to a drastic increase in resorufin production.[80] This side reaction would have not been observed in bulk samples at the same concentration, but segregation hindered diffusion, and allowed us to observe it (Figure 4n,o). The presence of fluorescein and HRP in the same GUV resulted in an unwanted, secondary reaction, which quenched one desired product, but at the same time improved the overall cascade efficiency, since enhancing the production of resorufin was the ultimate objective.

Finally, on the basis of a thorough investigation of the conditions to be avoided and to be exploited, the best arrangement naturally falls into complete co-encapsulation. By profiting from control over the inner GUV compositions that our microfluidic technique can offer, all three enzymes were easily co-encapsulated, while maintaining constant stoichiometry. Fluorescein production could be tuned by virtue of the proximity of enzymes and metabolites, which favored consumption of Amplex Red over fluorescein (Figure 4p). Moreover, the overall activity (i.e., the production of resorufin, in the last step) was remarkably improved, assisted partially by the oxidation of fluorescein to yield $\cdot$OH that in turn produced more resorufin (Figure 4q) (Movie S5, Supporting Information). With this arrangement, optimal conditions for maximum rates of production were accomplished.

We have developed a general strategy to study and optimize multi-step enzymatic reactions in synthetic confined spaces, based on biomimicry, and taking advantage of the high precision double emulsion technique. In this regard, an improved six-way junction geometry fabricated in silicon-glass devices, together with optimized fluid flow rates, provided a precise and high-throughput break-up of droplets in a single step, which guaranteed highly efficient biomolecular encapsulation and yielded 100% production of monodispersed double emulsions surrounded by a thin organic shell. These characteristics enabled the formation of GUVs, which constituted ideal supramolecular structures for insertion of biochannels. Accordingly, we demonstrated that the biopore, gramicidin, and the membrane protein, OmpF, preserved functionality when inserted in GUVs formed with the $PDMS_{26}$-*b*-$PMOXA_9$ block copolymer, whose membrane presented the required fluidity and flexibility to overcome the significant hydrophobic mismatch between its thickness and the formed pore. Moreover, the double emulsion technique allowed for an unprecedented control over the absolute and relative amounts of enzymes inside compartments, which besides enabling simultaneous co-encapsulation of three enzymes inside the cavity of single polymer GUV, allowed the presentation of high enzyme concentrations, in molecular proximity for optimizing the biochemical pathways. Overall, tailored cell-sized polymer GUVs, equipped with peptides/membrane proteins, and containing one or more types of encapsulated enzyme, were produced in a controlled manner as synthetic compartments that mimic elements of a complex cellular environment.

By mastering positional control of enzymes, we conducted a three-step cascade reaction in a variety of cascade topologies. A straightforward combinatorial study allowed special reaction effects to be identified which were not expected from model cascades based on well-known enzymes. Not only were we able to determine configurations to avoid, because of competing reactions, but more importantly we were able to establish the optimum reaction conditions, and to benefit from initially unwanted effects by enhancing the overall cascade efficiency and maximizing production of the final reaction product (resorufin). These important findings could not have been realized in a bulk reaction, nor in a single synthetic compartment of the same type, and highlights the necessity for working with multiple compartmentalization. In this respect, the current work provides a foundation for studying and optimizing cascade reactions only by physical means, much as cells do via subcellular segregation, without the time consuming and difficult work of varying relative enzymatic concentrations.

Our novel methodology described here can be applied to any multi-step cascade reactions, and offers the possibility of discovering unwanted pathways, determining the production of undesirable intermediates, and identifying other routes in which toxic products are rapidly consumed. These stages can all benefit from effective, controlled, and high-throughput processes, which ultimately can contribute to faster and cheaper results for improving the science and making new discoveries.

Experimental Section

Chemicals: Phosphate-buffered saline solution (Dulbecco's 1X PBS, without Ca^{2+}/Mg^{2+}) was purchased from BioConcept. Poly(vinyl alcohol) (PVA, M_w = 13–23 kDa), poly(ethylene glycol) (PEG, M_w = 6 kDa), poly(ethyleneimine) solution 50 wt% in H_2O, chloroform 99%, hexane anhydrous 95%, RGP, FGP, gramicidin from *Bacillus aneurinolyctus* (*Bacillus brevis*, gA), sucrose, carboxyfluorescein (CF), fluorescein isothiocyanate–dextran (FITC-dextran), potassium phosphate dibasic (K_2HPO_4), potassium phosphate monobasic (KH_2PO_4), and sodium chloride (NaCl) were obtained from Sigma-Aldrich and were used as received. Amplex Ultra Red (AR) was obtained from Invitrogen. Aquapel was obtained from PPG Industries. BODIPY 630/650 and the NHS

esters, Cy5, Oregon Green, and ATTO 550 were purchased from Thermo Fisher Scientific. Sodium Green (SG) was purchased from TEFLabs Inc.

Synthesis and Characterization of $PDMS_{26}$-b-$PMOXA_9$: The synthesis of the amphiphilic diblock copolymer poly(dimethyl siloxane)-*block*-poly(2-methyl-2-oxazoline) ($PDMS_{26}$-*b*-$PMOXA_9$) was conducted according to amended, previously reported protocols (Supporting Information).[47,48] Briefly, PDMS was synthesized by anionic ring opening polymerization of hexamethylcyclotrisiloxane (D_3), and the hydride-terminated PDMS-H was then transformed into monocarbinol-functionalized PDMS-OH with 2-allyloxyethanol. Activation for the following chain extension was done with trifluormethanesulfonic anhydride. Subsequently, 2-methyl-2-oxazoline (MOXA) was polymerized in a cationic ring-opening polymerization, followed by quenching with triethylamine and water. The average composition of the hydroxy-terminated copolymer was found to be $PDMS_{26}$-*b*-$PMOXA_9$, and corresponded to a molecular weight of M_n = 2800 g mol^{-1} determined by ^{1}H-NMR spectroscopy (Figure S3, Supporting Information). The molecular weight distribution was measured by gel permeation chromatography and showed a dispersity of Đ = 1.21 (Figure S4, Supporting Information).

OmpF Expression: The wild-type outer membrane protein F (OmpF) was obtained according to the same procedure already reported.[25]

Composition of Fluid Phases: The different compositions of IA, PO, and OA phases used in the experiments were as follows. Inner aqueous phase (IA): If not otherwise stated, all solutions were prepared with the starting composition of 20 w/v% of PEG and 300×10^{-3} M of sucrose in PBS solution (≈628 mOsm L^{-1}); 10×10^{-6} M carboxyfluorescein (CF) (Figure 2e–h); 198×10^{-6} M *β*-gal (l.h.s of Figure 3b); 0.25 mg mL^{-1} *β*-gal, 0.25 mg mL^{-1} GOx, and 0.5 μg mL^{-1} HRP (Figure 4a–c,f,h–q); 0.125 mg mL^{-1} *β*-gal, 0.125 mg mL^{-1} GOx (Figure 4d); 0.083 mg mL^{-1} *β*-gal, 0.083 mg mL^{-1} GOx, and 0.167 μg mL^{-1} HRP; 10×10^{-6} M Sodium Green (SG), 3×10^{-6} M gramicidin (gA) in buffer K (experiments aimed at detecting the signaling of the ion Na^+, Figure 3a); "buffer K" contained: 300×10^{-3} M of K_2HPO_4, 300×10^{-3} M of KH_2PO_4 added to 20 w/v% of PEG, and 300×10^{-3} M of sucrose in Milli-Q water (Milipore, resistivity of 18.2 MΩ cm^{-1}), at pH = 7.4. Polymer organic phase (PO): 6 mg mL^{-1} of $PDMS_{26}$-*b*-$PMOXA_9$ in 3:2 v/v hexane:chloroform solution. Outer aqueous phase (OA): if not otherwise stated, solutions were prepared with 5 w/v% of PVA in PBS solution (≈298 mOsm L^{-1}); 0.39×10^{-3} M OmpF (r.h.s. of Figures 3b,c and 4h–q). Collection phase (CP): If not otherwise stated, solutions were prepared with 700×10^{-3} M NaCl, 5 w/v% PVA in PBS solution (≈1628 mOsm L^{-1}); 700×10^{-3} M KCl, 5 w/v% PVA in buffer K solution (Figure 3a).

Operation of The Microfluidic Device: Immiscible fluids were infused into the microdevice (Figure 1) using a three module precision syringe pump (low pressure neMESYS, Cetoni). The fluid phases were fed at different flow rates, in particular, when conducting optimization of the double emulsion sizes (Figure 2). For all other experiments, the phases IA, PO, and OA were set to flow rates of 2, 1, and 50 μL min^{-1}, respectively. Double emulsion drops were prepared by one-step emulsification and collected for 10 min in a vial containing 200 μL of the CP solution, where they rapidly sank due to the difference in density caused by the addition of sucrose in the IA phase. Note that the difference in osmolarity created between IA phase and the solution surrounding the collected droplets was roughly 70 mOsm L^{-1}. Upon separation of the oil phase and dewetting up to equilibrium, polymer GUVs were produced.

Imaging: Double Emulsion Size Measurements: The microfluidic production of double-emulsion drops using a High Speed Digital Microscope (Meros, Dolomite) was recorded. A 5× objective equipped with a high-speed camera (1.3 megapixel colour camera, 1/2" CMOS sensor) was used to capture videos of double emulsions flowing in the main channel of the microchip, and these were further processed with the custom Matlab code to measure the droplet's inner core and outer shell diameters (the exact procedure is described in Supporting Information).

Imaging: GUV Functionalities and Size Measurements: GUVs were visualized in Nunc Lab-Tek eight-well chambers (Thermo Fisher Scientific, USA) using a Zeiss 880 CLSM microscope (Zeiss, Germany) with an objective (C-Apochromat 10× and 20×/1.2 W Korr FCS M27). To the suspension of GUVs (20 μL), together with a final concentration of 5×10^{-6} M of BODIPY 630/650 (5 μL), the following solutions were added to a total volume of 200 μL of collection phase (CP) in separated experiments, namely: i) 5×10^{-6} M RGP (Figure 3b), ii) 200×10^{-6} M of FITC-dextran (l.h.s of Figure 3c), iii) 200×10^{-6} M of CF (r.h.s of Figure 3c) and iv) 3.75×10^{-6} M FGP and 2.5×10^{-6} M Amplex Red (Movies S3–S5, Supporting Information). GUVs were imaged by BODIPY 630/650 staining the membrane to discriminate between hollow vesicles and eventual non separated organic phase droplets. For imaging GUVs, a 488 nm argon laser, a 561 nm DPSS 5561-10 laser, and a 633 nm HeNe laser were used. For CF, OregonGreen, and FITC-dextran, an argon laser (488 nm) was used, with 493–629 nm filters, MBS 488; for resorufin and ATTO 550, a DPSS (561 nm) laser was used, with 563–629 nm filters, MBS T80/R20; and for BODIPY and Cy5, a diode laser (633 nm) was used, MBS 488/561/ 633. The pinhole aperture was always 39 μm.

Images of GUVs acquired with the bright field were used for measuring GUV diameters via an image processing software written in Matlab (the exact procedure is described in Supporting Information).

Enzyme Labeling: Solutions of 2 mg mL^{-1} of *β*-gal, GOx, and HRP were prepared in PBS (pH adjusted to 8) and 3 molar equivalents of NHS ester reactive dyes: Cy5 (for *β*-gal), OregonGreen (for GOx), and Atto 550 (for HRP) were added. After an overnight reaction at room temperature, enzyme solutions were purified by centrifugation (Minispin Plus, Eppendorf) using filters (Amicon ultra 30 K, Merck) for 15 cycles of 5 min at maximum speed, using PBS as eluent. Subsequently, the resulting purified concentrate of labeled enzymes were diluted in the inner aqueous phase, containing 20 w/v% of PEG and 300×10^{-3} M of sucrose in PBS solution (75 μL in 500 μL) to obtain the solutions used for the formation of GUVs. The number of molecules of dye per number of molecules of enzymes was determined using fluorescent correlation spectroscopy (FCS). This method measures the fluctuations of the fluorescence intensity of fluorophores due to Brownian motion in femtoliter-sized confocal volumes. By dividing the counts per molecule (CPM, kHz) of labeled enzymes by the CPM of free dyes, an average number of 1.22 molecules of Cy5 per molecule of *β*-gal and 1.02 molecules of OregonGreen per molecule of GOx and 1.21 molecules of Atto 550 per molecule of HRP were obtained (Figure S8, Supporting Information). The remaining quantity of free dyes present in solution was also determined by FCS using a 2-component fit: only 0.27% of free Cy5, 1.7% of free Oregon green, and 0.53% of Atto 550 remained in solution.

Determination of the Confocal Volumes: To determine the amount of fluorescent-labeled enzymes encapsulated inside GUVs, the confocal volumes corresponding to both laser lines (488 and 633 channels) used to measure the fluorescent-labeled enzymes were calculated. To do so, solutions of fluorescent dyes with known diffusion coefficients—Atto 488 ($D = 4 \times 10^{10}$ m^2 s^{-1}) and Atto 655 ($D = 4.26 \times 10^{10}$ m^2 s^{-1})—were measured. Assuming that the confocal volume can be approximated by a 3D Gaussian shape, the temporal autocorrelation function can be measured, as follows:

$$G(t) = G_0\left(1+\frac{t}{\tau}\right)^{-1}\left(1+\frac{t}{\tau k^2}\right)^{-1/2} \quad (1)$$

Equation (1) results from the correlation of a time series, where G_0 is the correlation amplitude, k is the eccentricity of the confocal volume, and τ is the lag-time for which the correlation has dropped to half of its maximum. Thus, from the correlated data (corresponding to each dye) fitted with Equation (1), the structural parameters, $k = 5$, $\tau = 35$ μs for Atto 488, and $\tau = 54$ μs for Atto 655, were obtained (Figure S8, Supporting Information). The effective volumes V_{eff} for each dye (V_{eff} = 0.373 fL for the 488 line and V_{eff} = 0.784 fL for the 633 line) were calculated using

$$V_{eff} = k\left(4D\pi\tau\right)^{3/2} \quad (2)$$

Finally, the confocal volumes (V_{conf} = 0.132 fL for 488 line and V_{conf} = 0.227 fL for 633 line) were calculated using

$$V_{conf} = V_{eff}\left(\frac{1}{2}\right)^{3/2} \quad (3)$$

The lasers were used with 5% attenuation for the 488 line (ArgonRemote) and 10% attenuation for the 633 line (HeNe633), for the FCS measurements and the determination of confocal volumes.

Determination of the Concentration of Enzymes Inside GUVs: To determine the concentration of the enzymes in the solutions, the average number of particles present in the confocal volumes was also determined by FCS. Then knowing the number of enzymes present in the confocal volumes and the volume of the confocal volumes, the concentration of enzyme solutions was calculated and concentrations of 0.23 ± 0.01 mg mL^{-1} and 0.38 ± 0.01 mg mL^{-1} for the final solutions of β-gal and GOx, respectively, obtained. To determine the concentration of enzymes inside GUVs, brightness was measured via FCS in GUVs ($N = 3$) encapsulating one or two enzymes using a 2-component fit with a fixed diffusion time for each enzymes (Figure S9, Supporting Information). Knowing the volume of GUVs (approximately 3×10^4 fL), and using the same method as for the free enzyme solutions, the average number of enzymes in the confocal volumes were determined. The concentrations of enzymes per GUV were: 0.23 ± 0.02 mg mL^{-1} for β-gal and 0.38 ± 0.03 mg mL^{-1} 461 for GOx when encapsulated separately, and 0.11 ± 0.01 mg mL^{-1} for β-gal and 0.21 ± 0.01 mg mL^{-1} when co-encapsulated. The dilution factor (approximately 2) obtained for the co-encapsulation compared to separate encapsulation was consistent with the dilution of enzymes, and to account for it, concentrations of enzymes that were co-encapsulated in GUVs were multiplied by 2.

Monitoring Enzymatic Reactions: Enzymatic assays were performed using a Spectramax iD3 microplate reader (Molecular Devices, USA) in a 96-well, flat-bottomed black plate (Corning, USA) for fluorescence. Both β-gal and GOx were added to a final concentration of 12.5 µg mL^{-1} and HRP to a final concentration of 50 ng mL^{-1}, either encapsulated or free in solution, 3.75×10^{-6} M FGP, and 2.5×10^{-6} M Amplex Red and the volume was brought to 200 µL with the collection phase (PVA/PBS/NaCl). The production of fluorescein (from FGP) was followed at Ex: 485 nm Em: 525 nm, for resorufin (from Amplex Red) at Ex: 560 Em: 600 nm, every 30 s, for 20 min.

Supporting Information

Supporting Information is available from the Wiley Online Library or from the author.

Acknowledgements

The authors thank Dr. T. Pfohl (University of Freiburg) for the inspiration and fruitful discussions, and Dr. I. A. Dinu and Dr. P. Kong (University of Basel) for their assistance in drawing the reaction scheme. The authors gratefully acknowledge the financial support provided by the Swiss Nanoscience Institute, the Swiss National Science Foundation, the National Centre of Competence in Research–Molecular Systems Engineering (NCCR-MSE), and the University of Basel.

Conflict of Interest

The authors declare no conflict of interest.

Author Contributions

E.C.d.S. contributed to the formation of double emulsion templated GUVs; A.B. contributed to carrying out the cascade reactions; D.N. contributed to the development of the experimental setup; C.E.M. contributed to measuring the efficiency of enzymes encapsulation; D.S. contributed to the fabrication of the silicon-glass chips; R.W. contributed by synthesizing the block copolymer; E.L., C.G.P., and W.M. contributed to idealizing the concept of the work. The manuscript was written with the contributions of all authors. All authors gave approval to the final version of the manuscript.

Keywords

biochannels, double emulsion microfluidics, efficiency of encapsulation, multi-step cascade reactions, polymer giant unilamellar vesicles

Received: July 16, 2020
Revised: September 8, 2020
Published online: October 27, 2020

[1] D. Dziga, G. Zielinska, B. Wladyka, O. Bochenska, A. Maksylewicz, W. Strzalka, J. Meriluoto, *Toxins* **2016**, *8*, 76.
[2] P. K. Robinson, *Essays Biochem.* **2015**, *59*, 1.
[3] C. F. Megarity, B. Siritanaratkul, R. S. Heath, L. Wan, G. Morello, S. R. FitzPatrick, R. L. Booth, A. J. Sills, A. W. Robertson, J. H. Warner, N. J. Turner, F. A. Armstrong, *Angew. Chem., Int. Ed.* **2018**, *58*, 4948.
[4] J.-B. Lalanne, J. C. Taggart, M. S. Guo, L. Herzel, A. Schieler, G.-W. Li, *Cell* **2018**, *173*, 749.
[5] C. Hold, S. Billerbeck, S. Panke, *Nat. Commun.* **2016**, *7*, 12971.
[6] T.-Y. Dora. Tang, D. van Swaay, A. deMello, J. L. Ross Anderson, S. Mann, *Chem. Commun.* **2015**, *51*, 11429.
[7] Q. Xiao, S. S. Yadavalli, S. Zhang, S. E. Sherman, E. Fiorin, L. da Silva, D. A. Wilson, D. A. Hammer, S. André, H.-J. Gabius, M. L. Klein, M. Goulian, V. Percec, *Proc. Natl. Acad. Sci. USA* **2016**, *113*, E1134.
[8] M. Garni, T. Einfalt, R. Goers, C. G. Palivan, W. Meier, *ACS Synth. Biol.* **2018**, *7*, 2116.
[9] F. Itel, A. Najer, C. G. Palivan, W. Meier, *Nano Lett.* **2015**, *15*, 3871.
[10] D. Thalmeier, J. Halatek, E. Frey, *Proc. Natl. Acad. Sci. USA* **2016**, *113*, 548.
[11] C. E. Ashley, E. C. Carnes, G. K. Phillips, D. Padilla, P. N. Durfee, P. A. Brown, T. N. Hanna, J. Liu, B. Phillips, M. B. Carter, N. J. Carroll, X. Jiang, D. R. Dunphy, C. L. Willman, D. N. Petsev, D. G. Evans, A. N. Parikh, B. Chackerian, W. Wharton, D. S. Peabody, C. J. Brinker, *Nat. Mater.* **2011**, *10*, 389.
[12] J. G. Heddle, S. Chakraborti, K. Iwasaki, *Curr. Opin. Struct. Biol.* **2017**, *43*, 148.
[13] L. I. Kazakova, L. I. Shabarchina, G. B. Sukhorukov, *Phys. Chem. Chem. Phys.* **2011**, *13*, 11110.
[14] L. I. Kazakova, L. I. Shabarchina, S. Anastasova, A. M. Pavlov, P. Vadgama, A. G. Skirtach, G. B. Sukhorukov, *Anal. Bioanal. Chem.* **2013**, *405*, 1559.
[15] P. K. Harimech, R. Hartmann, J. Rejman, P. del Pino, P. Rivera-Gil, W. J. Parak, *J. Mater. Chem. B* **2015**, *3*, 2801.
[16] C. Hou, Y. Wang, H. Zhu, L. Zhou, *J. Mater. Chem. B* **2015**, *3*, 2883.
[17] L. Zhang, J. Shi, Z. Jiang, Y. Jiang, S. Qiao, J. Li, R. Wang, R. Meng, Y. Zhu, Y. Zheng, *Green Chem.* **2011**, *13*, 300.
[18] S. Kobori, N. Ichihashi, Y. Kazuta, T. Yomo, *Mol. BioSyst.* **2013**, *9*, 1282.
[19] Y. Tamba, T. Tanaka, T. Yahagi, Y. Yamashita, M. Yamazaki, *Biochim. Biophys. Acta, Biomembr.* **2004**, *1667*, 1.
[20] R. J. R. W. Peters, M. Marguet, S. Marais, M. W. Fraaije, J. C. M. van Hest, S. Lecommandoux, *Angew. Chem., Int. Ed.* **2014**, *53*, 146.
[21] S. Jeong, H. T. Nguyen, C. H. Kim, M. N. Ly, K. Shin, *Adv. Funct. Mater.* **2020**, *30*, 1907182.
[22] A. Küchler, M. Yoshimoto, S. Luginbühl, F. Mavelli, P. Walde, *Nat. Nanotechnol.* **2016**, *11*, 409.
[23] F. Itel, M. Chami, A. Najer, S. Lörcher, D. Wu, I. A. Dinu, W. Meier, *Macromolecules* **2014**, *47*, 7588.

[24] M. Lomora, M. Garni, F. Itel, P. Tanner, M. Spulber, C. G. Palivan, *Biomaterials* **2015**, *53*, 406.
[25] A. Belluati, I. Craciun, J. Liu, C. G. Palivan, *Biomacromolecules* **2018**, *19*, 4023.
[26] P. Tanner, O. Onaca, V. Balasubramanian, W. Meier, C. G. Palivan, *Chem. - Eur. J.* **2011**, *17*, 4552.
[27] P. Tanner, V. Balasubramanian, C. G. Palivan, *Nano Lett.* **2013**, *13*, 2875.
[28] S. Thamboo, A. Najer, A. Belluati, C. von Planta, D. Wu, I. Craciun, W. Meier, C. G. Palivan, *Adv. Funct. Mater.* **2019**, *29*, 1904267.
[29] C. Edlinger, T. Einfalt, M. Spulber, A. Car, W. Meier, C. G. Palivan, *Nano Lett.* **2017**, *17*, 5790.
[30] T. Trantidou, M. Friddin, Y. Elani, N. J. Brooks, R. V. Law, J. M. Seddon, O. Ces, *ACS Nano* **2017**, *11*, 6549.
[31] E. Amstad, S.-H. Kim, D. A. Weitz, *Angew. Chem., Int. Ed.* **2012**, *51*, 12499.
[32] S.-H. Kim, H. C. Shum, J. W. Kim, J.-C. Cho, D. A. Weitz, *J. Am. Chem. Soc.* **2011**, *133*, 15165.
[33] H. C. Shum, D. Lee, I. Yoon, T. Kodger, D. A. Weitz, *Langmuir* **2008**, *24*, 7651.
[34] M. Michelon, Y. Huang, L. G. [de la Torre], D. A. Weitz, R. L. Cunha, *Chem. Eng. J.* **2019**, *366*, 27.
[35] C. E. Meyer, J. Liu, I. Craciun, D. Wu, H. Wang, M. Xie, M. Fussenegger, C. G. Palivan, *Small* **2020**, 1906492.
[36] X. Xie, W. Zhang, A. Abbaspourrad, J. Ahn, A. Bader, S. Bose, A. Vegas, J. Lin, J. Tao, T. Hang, H. Lee, N. Iverson, G. Bisker, L. Li, M. S. Strano, D. A. Weitz, D. G. Anderson, *Nano Lett.* **2017**, *17*, 2015.
[37] G. T. Vladisavljevic, H. Shahmohamadi, D. B. Das, E. E. Ekanem, Z. Tauanov, L. Sharma, *J. Colloid Interface Sci.* **2014**, *418*, 163.
[38] L. R. Arriaga, S. S. Datta, S.-H. Kim, E. Amstad, T. E. Kodger, F. Monroy, D. A. Weitz, *Small* **2014**, *10*, 950.
[39] L. R. Arriaga, Y. Huang, S.-H. Kim, J. L. Aragones, R. Ziblat, S. A. Koehler, D. A. Weitz, *Lab Chip* **2019**, *19*, 749.
[40] E. Amstad, *Chimia* **2017**, *71*, 334.
[41] J. C. McDonald, G. M. Whitesides, *Acc. Chem. Res.* **2002**, *35*, 491.
[42] L. R. Arriaga, E. Amstad, D. A. Weitz, *Lab Chip* **2015**, *15*, 3335.
[43] A. Ładosz, P. R. von Rohr, *Chem. Eng. Sci.* **2018**, *191*, 398.
[44] S. Deshpande, Y. Caspi, A. E. C. Meijering, C. Dekker, *Nat. Commun.* **2016**, *7*, 10447.
[45] A. S. Utada, E. Lorenceau, D. R. Link, P. D. Kaplan, H. A. Stone, D. A. Weitz, *Science* **2005**, *308*, 537.
[46] A. R. Abate, J. Thiele, D. A. Weitz, *Lab Chip* **2011**, *11*, 253.
[47] S. Egli, M. G. Nussbaumer, V. Balasubramanian, M. Chami, N. Bruns, C. Palivan, W. Meier, *J. Am. Chem. Soc.* **2011**, *133*, 4476.
[48] D. Wu, M. Spulber, F. Itel, M. Chami, T. Pfohl, C. G. Palivan, W. Meier, *Macromolecules* **2014**, *47*, 5060.
[49] G. F. Christopher, N. Noharuddin, J. A. Taylor, S. L. Anna, *Phys. Rev. E: Stat., Nonlinear, Soft Matter Phys.* **2008**, *78*, 036317.
[50] S. A. Nabavi, S. Gu, G. T. Vladisavljević, E. E. Ekanem, *J. Colloid Interface Sci.* **2015**, *450*, 279.
[51] G. T. Vladisavljević, H. C. Shum, D. A. Weitz, in *UK Colloids 2011: An International Colloid and Surface Science Symposium* (Eds: V. Starov, P. Griffiths), Springer, Berlin, Germany **2012**, pp. 115–118.
[52] K. Kim, J. K. Lee, S. J. Han, S. Lee, *Appl. Sci.* **2020**, *10*, 1146.
[53] F.-C. Chang, Y.-C. Su, *J. Micromech. Microeng.* **2008**, *18*, 065018.
[54] P. Garstecki, M. J. Fuerstman, H. A. Stone, G. M. Whitesides, *Lab Chip* **2006**, *6*, 437.
[55] E. C. dos Santos, A. Ladosz, G. M. Maggioni, P. R. von Rohr, M. Mazzotti, *Chem. Eng. Res. Des.* **2018**, *138*, 444.
[56] D. F. do Nascimento, L. R. Arriaga, M. Eggersdorfer, R. Ziblat, M. d. F. V. Marques, F. Reynaud, S. A. Koehler, D. A. Weitz, *Langmuir* **2016**, *32*, 5350.
[57] N.-N. Deng, M. Yelleswarapu, W. T. S. Huck, *J. Am. Chem. Soc.* **2016**, *138*, 7584.
[58] C. Martino, S. Kim, L. Horsfall, A. Abbaspourrad, S. J. Rosser, J. Cooper, D. A. Weitz, *Angew. Chem.* **2012**, *51*, 6416.
[59] A. Belluati, S. Thamboo, A. Najer, V. Maffeis, C. von Planta, I. Craciun, C. G. Palivan, W. Meier, *Adv. Funct. Mater.* **2020**, *30*, 2002949.
[60] G. M. Cooper, *The Cell: A Molecular Approach*, 2nd ed., Sinauer Associates, Sunderland, MA, USA **2000**.
[61] M. Lomora, F. Itel, I. A. Dinu, C. G. Palivan, *Phys. Chem. Chem. Phys.* **2015**, *17*, 15538.
[62] M. Garni, S. Thamboo, C.-A. Schoenenberger, C. G. Palivan, *Biochim. Biophys. Acta, Biomembr.* **2017**, *1859*, 619.
[63] C. G. Palivan, R. Goers, A. Najer, X. Zhang, A. Car, W. Meier, *Chem. Soc. Rev.* **2016**, *45*, 377.
[64] T. Einfalt, M. Garni, D. Witzigmann, S. Sieber, N. Baltisberger, J. Huwyler, W. Meier, C. G. Palivan, *Adv. Sci.* **2020**, *7*, 1901923.
[65] A. Belluati, V. Mikhalevich, S. Yorulmaz Avsar, D. Daubian, I. Craciun, M. Chami, W. P. Meier, C. G. Palivan, *Biomacromolecules* **2020**, *21*, 701.
[66] X. Zhang, W. Fu, C. G. Palivan, W. Meier, *Sci. Rep.* **2013**, *3*, 2196.
[67] J. L. Kowal, J. K. Kowal, D. Wu, H. Stahlberg, C. G. Palivan, W. P. Meier, *Biomaterials* **2014**, *35*, 7286.
[68] S.-H. Kim, J. W. Kim, D.-H. Kim, S.-H. Han, D. A. Weitz, *Microfluid. Nanofluid.* **2013**, *14*, 509.
[69] J. Xie, Z. Liang, Y.-C. Lu, *Nat. Mater.* **2020**.
[70] A. Armada-Moreira, B. Thingholm, K. Andreassen, A. M. Sebastião, S. H. Vaz, B. Städler, *Adv. Biosyst.* **2018**, *2*, 1700244.
[71] D. H. Juers, B. W. Matthews, R. E. Huber, *Protein Sci.* **2012**, *21*, 1792.
[72] E. C. Adams, R. L. Mast, A. H. Free, *Arch. Biochem. Biophys.* **1960**, *91*, 230.
[73] M. Ghafari, A. Mashaghi, *Phys. Chem. Chem. Phys.* **2017**, *19*, 25168.
[74] J. Ma, A. Shojaie, G. Michailidis, *BMC Bioinf.* **2019**, *20*, 546.
[75] G. Buzi, J. Doyle, *49th IEEE Conf. on Decision and Control (CDC)*, IEEE, Piscataway, NJ, USA **2010**, p. 4697.
[76] L. Schoonen, J. C. M. van Hest, *Adv. Mater.* **2016**, *28*, 1109.
[77] K. Kleppe, *Biochemistry* **1966**, *5*, 139.
[78] K.-S. Shin, H.-D. Youn, Y.-H. Han, S.-O. Kang, Y. C. Hah, *Eur. J. Biochem.* **1993**, *215*, 747.
[79] S. Pirillo, F. S. G. Einschlag, M. L. Ferreira, E. H. Rueda, *J. Mol. Catal. B: Enzym.* **2010**, *66*, 63.
[80] D. Debski, R. Smulik, J. Zielonka, B. Michałowski, M. Jakubowska, K. Dębowska, J. Adamus, A. Marcinek, B. Kalyanaraman, A. Sikora, *Free Radicals Biol. Med.* **2016**, *95*, 323.